Towards high-throughput DNA synthesis in a silicon-based MEMS 'virtual thermal well'-array

V. Narayan[1], A. Ferguson[1], Y.-C. Lin[1], B. Kirkpatrick[1], M. Hayes[1], A. Prak[2]

1. Evonetix Ltd., Little Chesterford, United Kingdom
2. Lionix International Ltd., Enschede, The Netherlands

Abstract: At Evonetix we are developing a silicon MEMS chip with a large number of reaction sites that operate in parallel to synthesise DNA. Each reaction site consists of an electrical heater on a SiO_2 membrane supported by SiO_2 pillars. The heater is passivated by a dielectric layer and capped with gold to host the chemistry. There are approximately 10 heaters per mm^2, electrical connections to which are made using through-silicon-vias. Fluid flows over the heaters and is used to transport chemical reagents. In this manuscript we describe our use of COMSOL to design the reaction site and associated heat pathways in order to have temperature uniformity across a reaction site, minimal crosstalk between neighbouring sites, and robustness of the temperature profile to a flowing fluid environment. We find excellent agreement between simulations and experimentally measured values.

1. Introduction

Evonetix is a Cambridge-based start-up company working on a revolutionary new technology to synthesise high-fidelity DNA at scale. Our technology is based on a chip with a large number of reaction sites that facilitate multiple parallel synthesis channels. We operate a modified phosphoramidite cycle on these sites and combine with a proprietary error-detection scheme to enhance yield. Within this modified phosphoramidite process temperature can be used to accelerate or decelerate reaction rates to the extent that reactions can be 'switched on/off'. Therefore, a central requirement of our synthesis process is the precise control of temperature.

Our approach is based on a Si MEMS chip in which multiple reaction sites can be controlled independently. The reaction sites operate within a common fluidic environment and are turned on/off by adjusting their temperature. This temperature control results in the creation of distinct *thermal wells* – fluid volumes whose temperature can be controlled precisely and independently even without physical separating barriers, and under conditions of moderate fluid-flow. The DNA grown on these are then scanned for errors which are removed prior to combining the DNA segments into longer sequences.

2. Experimental Set-up

The individual reaction sites (figure 1) consist of a heater on a SiO_2 membrane supported by SiO_2 pillars. The regions between the SiO_2 membranes are bulk Si. In the figure we define three regions within the unit site: i) the gold reaction site that hosts the biochemistry; ii) the 'guard region' or the region of the membrane outside the reaction site; and iii) the 'passive region' between the membranes. The heaters are protected from the fluid using a passivation layer on top of which is a gold pad that hosts the biochemistry. Liquid containing chemical reagents is flowed over the reaction sites and chemical reactions occur or not depending on the site temperature.

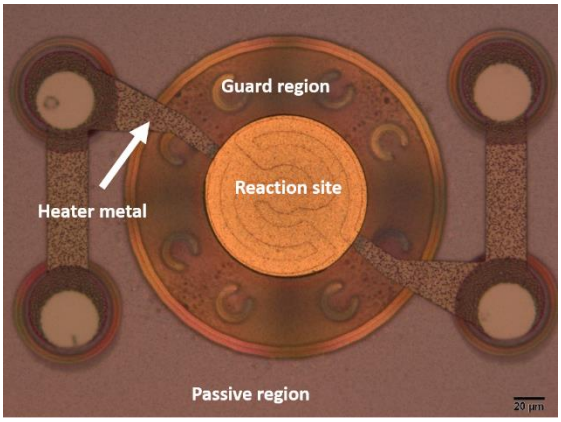

Figure 1. Optical image of a unit site of our silicon MEMS DNA synthesis platform. The reaction site is gold, the guard region is a SiO_2 membrane supported by SiO_2 pillars, and the passive region is bulk silicon. The heater trace can be seen under the reaction site gold with external leads for a four-wire measurement.

3. Simulation

We simulated the system in COMSOL with a view to identify the optimum geometrical configuration that would yield:

1. Well-defined thermal wells that are robust to reasonable rates of fluid flow.

2. Highly uniform spatial temperature profile across the reaction site.
3. Minimal cross-talk between sites, i.e., the ability to tune the sites independent of one another.

Figure 2 shows the geometry being simulated as rendered within COMSOL. The figure shows a single unit which is repeated in the experimental geometry. We used the ECAD import module to directly import the heater structure prepared in GDS format (compatible with manufacturer's requirements). All simulations were performed using realistic material parameters obtained from the in-built materials and using external literature sources.

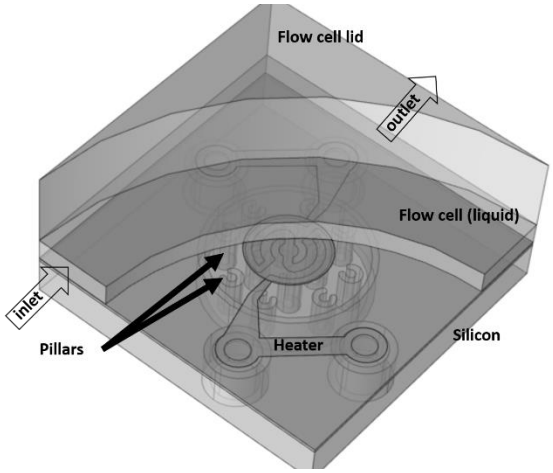

Figure 2. Geometry that was simulated within COMSOL. The top layers (flow cell and lid) are partially cut out for clarity.

We used the *Heat Transfer* package to study the steady-state and transient thermal response of our system. The temperature is tuned by passing a current through the heater and this was modelled using the *electromagnetic* (Joule) *heating* coupling. This was then extended to study the effect of flowing fluid using the *Laminar Flow* package with *non-isothermal flow* coupling. A flow inlet and outlet were defined as shown in figure 2.

The equations governing the steady-state temperature distribution of the system are as follows:

$$\rho C_p \mathbf{u}\cdot\nabla T + \nabla\cdot\mathbf{q} = Q \qquad (1)$$

Here ρ is the density of the medium, C_p is the heat capacity of the medium, $\mathbf{u}$ is the velocity of the medium (non-zero only in the region of liquid flow), T is the temperature of the medium (and the dependent variable being solved for), $\mathbf{q}$ is the heat flux given by:

$$\mathbf{q} = -\kappa\nabla T \qquad (2)$$

where κ is the thermal conductivity of the medium. The right side in Eq. 1 represents the power input per unit volume to the system which in this case is through Joule heating:

$$Q = \mathbf{J}\cdot\mathbf{E} \qquad (3)$$

where $\mathbf{J}$ is the electric current density and $\mathbf{E}$ is the electric field. By construction $\mathbf{J}$ and $\mathbf{E}$ are only non-zero in the heater and heater leads (which are electrically isolated from the rest of the setup in our devices using dielectric passivation layers). However, the *Joule Heating* multiphysics coupling is applied to the entire system, and this is sufficient to obtain accurate predictions of T.

To model the flow of liquid across the reaction site we used the *Laminar Flow* module which is justified by the low Reynolds number (Re ≈ 0.03). The corresponding equations read:

$$\rho(\mathbf{u}\cdot\nabla\mathbf{u}) = \nabla\cdot[-p\mathbf{I} + \mu(\nabla\mathbf{u} + (\nabla\mathbf{u})^T)] \qquad (4)$$

$$\rho\nabla\cdot\mathbf{u} = 0 \qquad (5)$$

where p is the pressure of the fluid and μ is its viscosity.

The boundary conditions employed are:

1. The flow cell lid was maintained at ambient temperature.
2. The bottom plane of the simulation geometry was held at a fixed temperature of 10 °C to emulate the action of a thermoelectric cooler connected to the bottom of the Si chip.

Apart from this, the system was considered to be thermally isolated.

4. Results: comparing simulation results to experimental findings

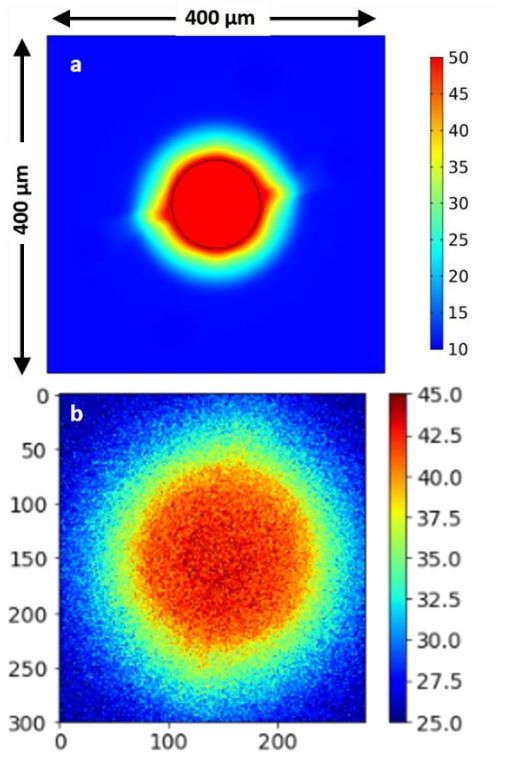

Figure 3. Comparison of the simulated (a) and experimentally measured (b) surface temperature profiles at the reaction site.

In this section we will compare the results of our simulations to experimentally measured values. Measurements were performed on prototype chips designed based on the simulation and fabricated at Lionix International, The Netherlands. Figure 1 shows an optical image of one of the devices reported here.

Figure 3a shows the steady-state temperature distribution on the surface of the reaction site when 6 mW of power is dissipated through the heater. Visually it is clear that there is excellent temperature uniformity, with the most significant deviations occurring at the location of the heater leads. The normalised standard deviation of the temperature distribution over the reaction site surface is less than 3%.

In figure 3b we show our measurements of the surface temperature profile using an epifluorescence microscopy. Here 6 mW was dissipated through the heater which is similar to that used in the model. The data was collected with the flow cell filled with a solution of rhodamine B (RhB), a fluorescent molecule whose fluorescence intensity depends upon temperature (over the range of temperatures relevant to our experiments the intensity of RhB increases by about 1.5% for a 1 °C decrease in the temperature). The top right plot shows the inferred temperature based on a linear mapping of intensity to temperature.

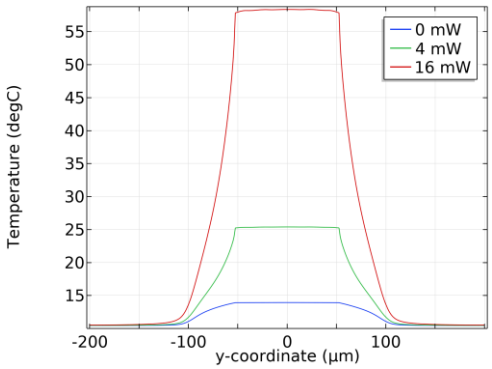

Figure 4. The temperature of the reaction site ($|r| < 50$ µm) and passive regions ($|r| > 100$ µm) are largely constant and irrespective of power, the temperature gradient is sustained only in the guard region (50 µm $< |r| <$ 100 µm).

The experimental findings confirm the model predictions of a well-formed thermal well with uniform temperature across the reaction site that decays over the guard region and settles to an approximately constant 25 °C in the passive region, which was the ambient temperature on the day of measurement.

Figure 4 shows the temperature profile along the reaction site surface for a range of voltages across the heater. It is seen that the reaction sites are sharply defined and, importantly, the temperature outside the guard region ($|r| > 100$ µm, see axis label) is negligibly affected by the heat dissipated in the heater. In other words, the simulations predict the crosstalk between sites to be negligible, and this has been experimentally verified by us. The data also enables an estimation of the 'thermal resistance' (R_{th}) of the system, defined as the temperature increase at the reaction site (ΔT) per unit power dissipated in the heater (P). As shown in figure 5 the measured and simulated values of R_{th} are in excellent agreement.

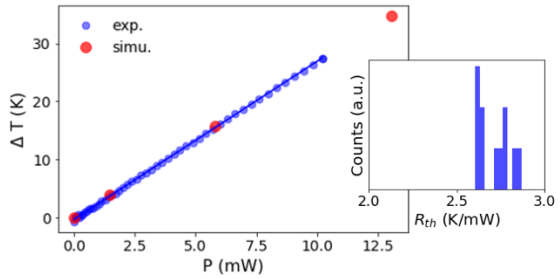

Figure 5. The experimentally determined and simulated dependence of temperature rise (Δ*T*) with power (*P*) are in excellent agreement. The inset shows a histogram of R_{th} values extracted from measurements on 11 devices.

In figure 6 we examine the effect of flowing liquid across the site. We observe that for average flow rates up to 1 mm/s there is no perceptible change in the profile of the thermal well and, therefore, in the value of R_{th}. We confirm these in experiments where we see no discernible change in the surface temperature profile upon increasing the flow rate to 1 mm/s. Importantly, this is approximately the maximum flow rate we expect to use in our synthesis experiments. At higher rates the fluid advects heat which distorts the temperature profile and reduces the average R_{th} across the site.

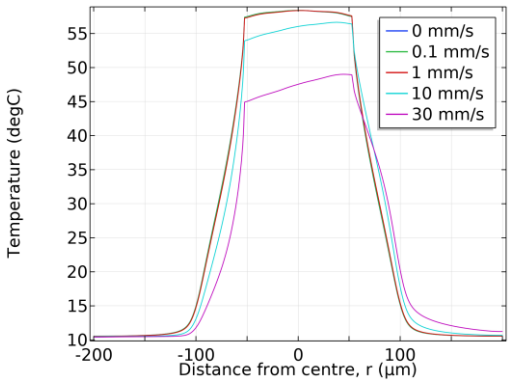

Figure 6. Upon increasing the flow rate through the cell there is initially no change in the temperature profile (traces for *u* = 0 mm/s, 0.1 mm/s, and 1 mm/s completely overlay on each other and cannot be discerned in the plot). At even higher velocities, the average temperature of the site decreases and the temperature profile becomes asymmetric along the direction of flow (along the positive *r*).

5. Discussion

In this section we discuss the roles of the materials and geometry of the setup towards achieving the desired attributes. The first criterion, namely that of tightly confined thermal wells that operate without cross-talk even under conditions of flow, was satisfied due to the combination of an almost thermally isolated membrane surrounded by a strongly thermally conductive bulk Si region. The relatively small thermal conductance of the SiO_2 membrane implies that it can sustain a temperature gradient, whereas in contrast, the high thermal conductivity Si remains essentially at a fixed temperature thereby serving to isolate the membranes from one another. This is also seen to hold true for moderate flow rates where the heat transported by the flow away from a site is overwhelmed by the heat injected from the heater as well as that drawn away by the Si substrate.

The SiO_2 pillars also contribute to the management of thermal pathways in the system, but their role is two-fold: first, they render the region below the membrane with an effective thermal conductivity which is lower than that of SiO_2 (by virtue of the of the fact that they partially fill this volume). This effective thermal conductivity provided an optimum thermal isolation such that the reaction site can be heated, but also responds quickly to power being switched on/off. Second, the pillars provide mechanical stability to the thin membrane, and prevent it from flexing during operation.

While the above considerations contribute to the formation of the thermal wells, we are also interested in the temperature uniformity across the reaction site. This was achieved by optimising the shape of the heater track such that more heat is dissipated at its periphery where it is closer to the 'cold' Si. This served to suppress long wavelength variations across the reaction site. There are, however, short wavelength variations that arise in this design inherently due to the meandering track, between the arms of which there is no power dissipated. To smooth these out, we increased the thickness of the reaction site gold which then acts as a 'heat spreader'. The final geometry is a combined optimisation of these two.

6. Conclusions

In conclusion, we have made effective use of COMSOL to predict and tune the properties of our experimental system, prototypes of which were manufactured whose performance matched very well with the simulations. In particular, we have been able to fine tune the geometry whilst working within constraints of manufacturability, availability of materials, and cost. We now aim to conduct system-level investigations of MEMS platform integrating with biochemistry, preliminary work of which is ongoing using the *Chemicals Engineering* module.